Detecting charge and lattice dynamics in photoinduced charge-order melting in perovskite-type manganites using a 30-femtosecond time resolution

Hiroyuki Matsuzaki,[1] Hirotaka Uemura,[1] Masakazu Matsubara,[2] Tsuyoshi Kimura,[3,*] Yoshinori Tokura,[2,3] and Hiroshi Okamoto[1,2,4,†]

[1]*Department of Advanced Materials Science, University of Tokyo, Kashiwa, Chiba 277-8561, Japan*

[2]*National Institute of Advanced Industrial Science and Technology (AIST), Tsukuba, Ibaraki 305-8562, Japan*

[3]*Department of Applied Physics, University of Tokyo, Tokyo 113-8856, Japan*

[4]*CREST–JST, Kawaguchi, Saitama 332-0012, Japan*

(Received 13 April 2009; revised manuscript received 31 May 2009; published 24 June 2009)

We investigated the ultrafast dynamics of photoinduced melting of charge and orbital order in a perovskite-type manganite, $Nd_{0.5}Ca_{0.5}MnO_3$, by means of pump-probe reflection spectroscopy. By irradiation with a 20-fs laser pulse, only the charge sectors become melted within ~30 fs through strong electron correlations. During this process the oxygen displacements associated with the ordered phase persist. These displacements are subsequently released accompanied by several coherent oscillations. The coherent oscillation corresponding to the Jahn-Teller mode has relatively large amplitude demonstrating that the orbital order plays a significant role on the stabilization of the charge order.

DOI: 10.1103/PhysRevB.79.235131 PACS number(s): 78.47.J−, 75.47.Lx, 78.30.−j, 78.40.Ha

I. INTRODUCTION

Recent studies on strongly correlated electronic systems have unveiled various intriguing phenomena due to the strong interplay among charge, spin, orbital, and lattice degrees of freedom.[1,2] One such example is colossal magnetoresistance in perovskite-type manganites, which originates from the competition between the antiferromagnetic charge-order insulator phase and the ferromagnetic-metal phase.[3] Namely, the melting of the charge order and the appearance of the ferromagnetic-metal phase under magnetic fields are the fundamental origins of this magnetoresistance.

Most of the manganites, $RE_{1-x}AE_xMnO_3$ (RE: rare-earth ions, AE: alkaline-earth ions), with small bandwidth exhibit a characteristic ordering pattern called the charge-exchange (CE) type at near half doping levels ($x \sim 0.5$).[4,5] Below the critical temperature (T_{CO}), a checkerboard-type charge order with alternating Mn^{3+}/Mn^{4+} sites or equivalently $3d$ e_g^1/e_g^0 configuration and a zigzag-chain-type order of $3x^2-r^2$ and $3y^2-r^2$ orbitals, referred to as the orbital order, appear as depicted in Fig. 1(a). Below the Néel temperature (T_N), the spins of $3d$ electrons are ordered ferromagnetically along the orbital zigzag chain and antiferromagnetically between the chains.

The charge order is considered to be stabilized mainly by the intersite Coulomb repulsion of e_g electrons. That is, charges are ordered so that the Coulomb repulsion energy among $3d$ electrons in different sites is decreased. From theoretical studies, it was pointed out that the orbital-orbital coupling, the Jahn-Teller (JT) and breathing-type oxygen distortions, and the double-exchange interaction along ferromagnetic chains also play key roles in the stabilization of CE-type charge-order phase.[6–12] It is, however, difficult to extract each contribution to the stabilization of the charge order from the generally used steady-state measurements such as x-ray diffraction, Raman-scattering, spin-susceptibility, and transport measurements, since a combination of complicated interactions gives rise to the ordered phase. Thus, the stabilization mechanism of the charge- and orbital-order phase in manganites has not been fully understood to date.

In order to solve this problem, transient optical spectroscopy with a femtosecond (fs) laser pulse is a powerful tool. It enables us to determine the dominant interactions between charge, spin, orbital, and lattice sectors by isolating the response of each sector in the time domain. To get precise information about each sector in this framework, it is necessary to perform the measurement with a very low excitation density, in which complex nonlinear phenomena under strong excitations can be excluded. The ultrafast time reso-

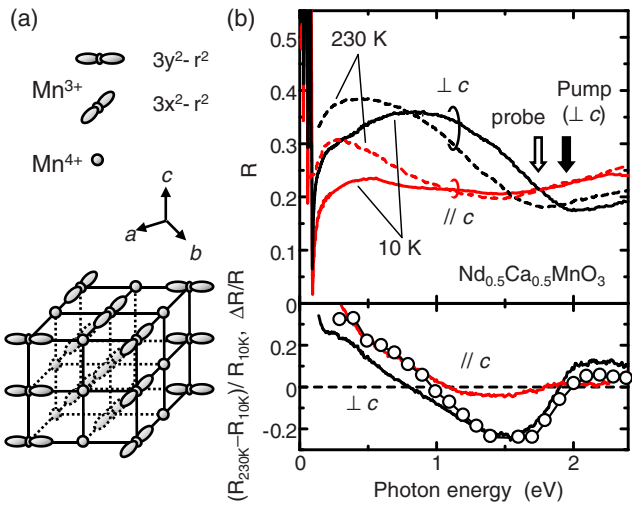

FIG. 1. (Color online) (a) Schematic illustrations of charge and orbital order in $Nd_{0.5}Ca_{0.5}MnO_3$. (b) Upper panel: reflectivity spectra for $E \| \mathbf{c}$ and $E \perp \mathbf{c}$ at $T=10$ K (solid lines) and $T=230$ K (broken lines) (Ref. 20). Lower panel: spectra of photoinduced reflectivity change ($\Delta R/R$) (open circles) for $E \perp \mathbf{c}$ at $T=10$ K with the pump energy of 1.55 eV and the excitation photon density of 0.01 ph/Mn, and differential reflectivity spectra $[(R_{230\ K}-R_{10\ K})/R_{10\ K}]$ (Ref. 16).

lution is also indispensable to detect the dynamics of oxygen displacements, which play important roles in the stabilization of both charge and orbital order. Typical frequencies and periods of oxygen vibrations relevant to charge and orbital order in manganites are ~600–200 cm^{-1} and ~60–170 fs, respectively, so that a time resolution of ~30 fs or less is necessary. In addition, the use of a half-doped system ($x=0.5$) allows the relevant physics to be simplified.

For the present study, we selected a typical half-doped manganite, $Nd_{0.5}Ca_{0.5}MnO_3$ ($T_{CO}=250$ K and $T_N=150$ K) and performed pump-probe reflectivity measurements with a ~20-fs laser pulse (~30-fs time resolution) and ultrahigh sensitivity. We succeeded in detecting small reflectivity changes using an excitation photon density of less than 10^{-3} photon/Mn. The results revealed that the laser pulse melts only the order of the charge sector within ~30 fs through strong electron correlation. Subsequently, the oxygen displacements associated with the charge order are released accompanied by several kinds of coherent oscillations. In particular, the coherent oscillation of the JT mode has a large amplitude suggesting that the orbital order coupled with the JT mode plays a significant role in the stabilization of the charge order.

The response to a laser pulse has been studied in manganites from the viewpoint of photoinduced phase control. Photoinduced melting of the charge order by a nanosecond laser pulse was first achieved in $Pr_{0.7}Ca_{0.3}MnO_3$ under a static external electric field.[13] Subsequently, attempts to control the charge-order phase of manganites were performed with a fs laser pulse in the absence of an external electric field. In fact, not only photoinduced melting of charge order[14–18] but also a photoinduced transition from a charge-order phase to a ferromagnetic-metal phase has been achieved.[19] In these studies, a strong excitation with a photon density larger than 0.01 photon/Mn has been used. Our approach based upon extremely weak photoexcitation and high time resolution, which is fundamentally different from those previously reported, can give significant insights into the stabilization mechanism of charge and orbital order.

II. EXPERIMENTAL DETAILS

A single crystal of $Nd_{0.5}Ca_{0.5}MnO_3$ was grown by the floating-zone method.[20] The as-grown crystal was cut to obtain a pseudocubic (100) surface and then annealed at 1000 °C in flowing O_2 gas after polishing.

In the measurement of the transient photoinduced change ($\Delta R/R$) in reflectivity (R), a pump-probe method was used. Pump and probe pulses were provided by two noncollinear optical parametric amplifiers, both of which were excited with the output of a Ti:sapphire regenerative amplifier [795 nm (1.56 eV), duration of 130 fs, and repetition rate of 1 kHz]. The typical pulse width of the outputs of the noncollinear optical parametric amplifiers was 20 fs. The delay time t_d of the probe pulse relative to the pump pulse was adjusted by changing the path length of the pump pulse. The zero-time delay and the instrumental response function were determined by the sum-frequency cross correlation between the pump and probe pulses using a β-BaB_2O_4 crystal. The width of the instrumental response function corresponding to the time resolution of the system was ~30 fs.

III. RESULTS AND DISCUSSION

In Fig. 1(b) (upper panel), we display the reflectivity spectra of $Nd_{0.5}Ca_{0.5}MnO_3$ for a light polarization (E) parallel ($\parallel$) and perpendicular ($\perp$) to the **c** axis at 10 K ($\ll T_{CO}$) and 230 K ($\leq T_{CO}$). The spiky structures in the infrared region below 0.08 eV are due to optical-phonons mode. At 10 K, the reflectivity spectra show strong polarization dependence reflecting the anisotropic electronic structure in the CE-type charge and orbital order. The broad structure at 0.2–2 eV for $E\perp\mathbf{c}$ at 10 K is assigned to the transition from Mn^{3+} to Mn^{4+}. In contrast, at 230 K just below T_{CO}, the spectral weight for $E\perp\mathbf{c}$ shifts to the lower energy and the optical anisotropy is suppressed compared to 10 K due to the weakening of charge and orbital order.[16] The solid lines in the lower panel of Fig. 1(b) show the differential spectrum $[(R_{230\ K}-R_{10\ K})/R_{10\ K}]$ of the reflectivity spectra at 230 K ($R_{230\ K}$) and 10 K ($R_{10\ K}$), which correspond to the spectral change induced by the collapse of charge and orbital order. The previous pump-probe study with a ~200-fs time resolution suggested that charge and orbital order is melted by a photoexcitation with an excitation photon density of 0.01 photon(ph)/Mn due to the similarity between the differential reflectivity $[(R_{230\ K}-R_{10\ K})/R_{10\ K}]$ spectrum and the photoinduced reflectivity-change ($\Delta R/R$) spectrum shown by open circles in Fig. 1(b) (lower panel).[16] Therefore, the time dependence of $\Delta R/R$ is considered to directly reflect the dynamics of photoinduced melting of charge and orbital order.

In Fig. 2, we show the time profiles of $\Delta R/R$ at 1.72 eV for $E\parallel\mathbf{c}$ and $E\perp\mathbf{c}$ measured with a time resolution of ~30 fs. To excite the Mn^{3+} to Mn^{4+} transition, the energy and the polarization of the pump light (E_{ex}) are set at 1.94 eV and $E_{ex}\parallel\mathbf{c}$, respectively. The excitation photon density (x_{ph}) is 6.5×10^{-3} ph/Mn. Immediately after the photoirradiation, reflectivity at 1.72 eV decreases for both polarizations, indicative of the melting of charge order. Following this initial drop, a coherent oscillation is observed, especially for $E\perp\mathbf{c}$.

To examine the initial dynamics in more detail, in Fig. 3(a) we compare the expanded time profiles of $\Delta R/R(E\perp\mathbf{c})$ with a normalized scale for several values of x_{ph} (lower part) together with the cross correlation of the pump and probe pulses (upper part). The full width at half maximum of the cross correlation is 33 fs. It can be seen that the initial dynamics of the reflectivity decrease due to the melting of the charge order is independent of x_{ph} and occurs with *no time delay*. That is, the charge order is melted much faster than the time resolution of 33 fs. Figure 3(b) shows the excitation photon-density (x_{ph}) dependence of $|\Delta R/R|$ at $t_d=40$ fs, which is proportional to x_{ph} up to 2×10^{-3} ph/Mn and then tends to saturate. By comparing the magnitude of $\Delta R/R$ in the linear region ($x_{ph}<2\times10^{-3}$ ph/Mn) with the differential relativity $[(R_{230\ K}-R_{10\ K})/R_{10\ K}]$ shown in Fig. 1(b), the size of the domain in which charge and orbital order is melted was evaluated to be ~140 Mn sites per photon.

Next, we analyzed the overall time profile of $\Delta R/R$ at 1.72 eV shown in Fig. 2. For $E\perp\mathbf{c}$ the time profile consists

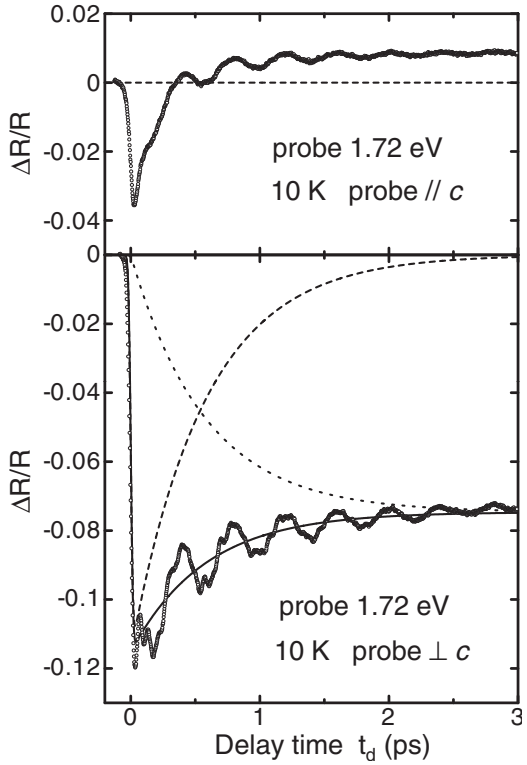

FIG. 2. Time evolutions of $\Delta R/R$ (open circles) for a probe energy of 1.72 eV for $E\|\mathbf{c}$ (the upper panel) and $E\perp\mathbf{c}$ (the lower panel) at 10 K. The pump energy is 1.94 eV($E\perp\mathbf{c}$) and the excitation photon density is 6.5×10^{-3} ph/Mn. The solid line represents the result of fitting. The broken and the dotted line denote the fast and slow component, respectively (see text).

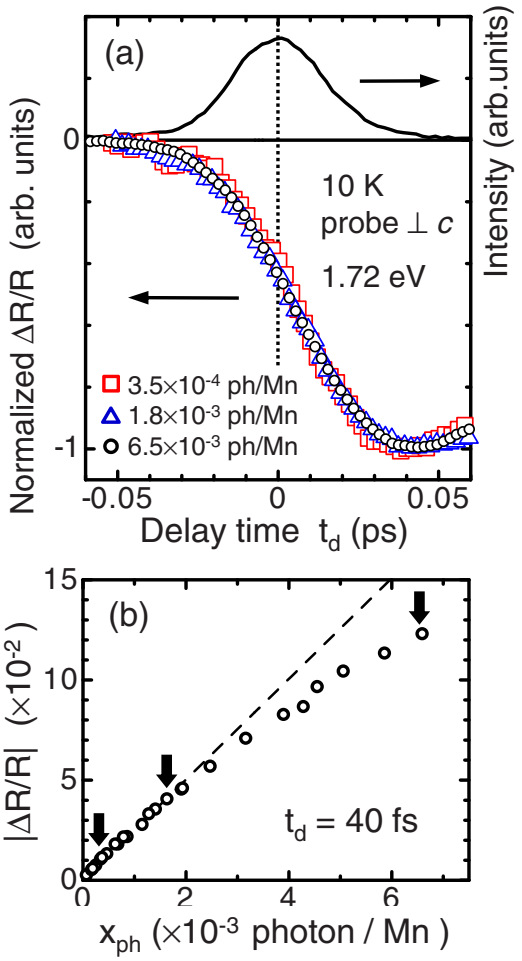

FIG. 3. (Color online) (a) Time profile of $\Delta R/R$ observed at the probe energy of 1.72 eV for $E\perp\mathbf{c}$ at 10 K for the three excitation photon densities x_{ph} marked by the solid arrows in (b) (lower panel) and the cross-correlation profile between pump (1.94 eV) and probe (1.72 eV) pulses (upper panel). (b) x_{ph}-dependence of $|\Delta R/R|$ at t_d=40 fs.

of two components; an ultrafast component decaying within $t_d\sim1$ ps and a slower one which dominates $\Delta R/R$ for $t_d>1$ ps. The time profile for $E\|\mathbf{c}$ also seems to include two components with similar time constants, although the sign of the slower component is positive. To analyze these components, the background time profile excluding the oscillation signals for $E\perp\mathbf{c}$ at 1.72 eV was fitted by the following formulas consisting of the two terms:

$$I(t) = I_1 \exp(-t/\tau_0) + I_2\{1-\exp(-t/\tau_0)\}. \quad (1)$$

The first term corresponds to the photocarrier-induced changes in the system and its recovery and the second to the thermalization process of electron-spin-lattice-coupled system.[14,16,18] By using this formula, the background time profile could be well reproduced as shown by the solid line in the lower panel of Fig. 2. The first and second terms are indicated by the broken and dotted lines, respectively. In the fitting procedure, the response function of the measurement system shown in the upper panel of Fig. 3(a) was taken into account as a Gaussian profile. The obtained value of τ_0 is 0.6 ps, which corresponds to the characteristic time for the recovery of the charge order.

The oscillatory component for $E\perp\mathbf{c}$ at 1.72 eV (10 K) obtained by subtraction of the background component mentioned above is plotted in Fig. 4(a) by open circles. The initial profile up to t_d=0.3 ps is also shown in Fig. 4(b). The data were analyzed assuming the sum of four damped oscillators given by the following formula:

$$\Delta R_{\mathrm{osc}}/R = \sum_{i=1}^{4} A_i \cos(\omega_i t - \phi_i)\exp(-t/\tau_i), \quad (A_i>0), \quad (2)$$

where A_i is the oscillation amplitude, ω_i is the oscillation frequency, τ_i is the decay time, and ϕ_i is the initial phase. In the fitting procedure, the response function of the measurement system was again taken into account as a Gaussian profile. The simulated profile reproduces the experimental result well as shown by the solid lines in Figs. 4(a) and 4(b). The four components are also shown in the lower parts of the figures. The evaluated frequencies ω_i of the four modes are 82, 224, 339, and 469 cm^{-1}. The fitting parameters are summarized in Table I. The initial phases ϕ_i are almost equal to zero for each oscillation indicating that the oscillations are cosinusoidal.[21] This suggests that the observed coherent oscillations are attributable not to the impulsive stimulated Ra-

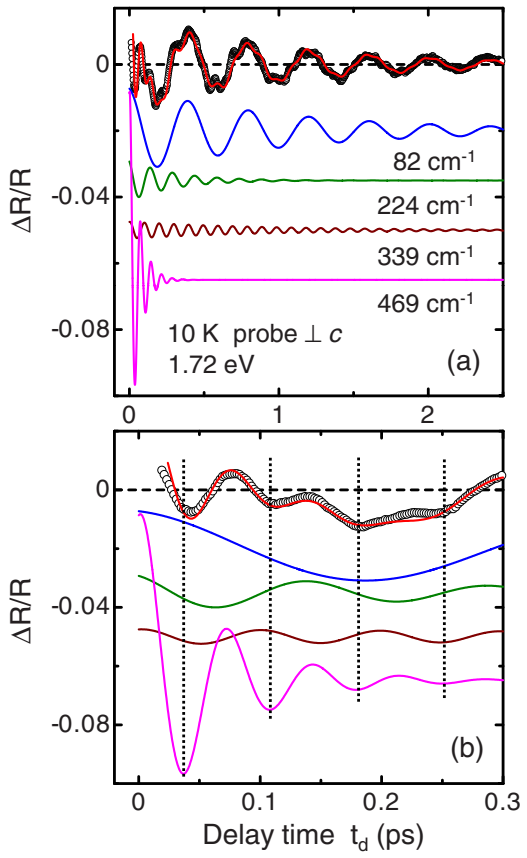

FIG. 4. (Color online) [(a) and (b)] Oscillatory component (open circles) extracted from the time profile of $\Delta R/R$ for $E \perp \mathbf{c}$ at 10 K (lower panel of Fig. 2). The solid line is a fitting curve, which is the sum of the four damped oscillators shown in the lower parts.

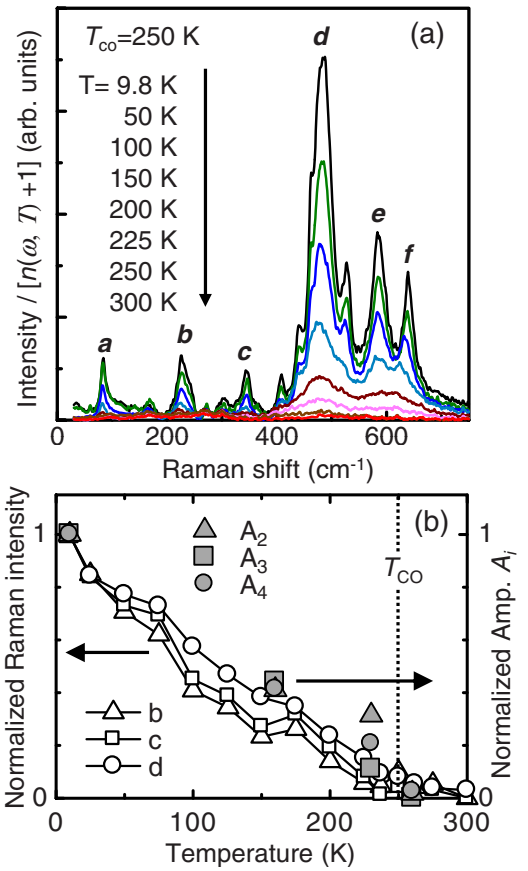

FIG. 5. (Color online) (a) Temperature dependence of the Raman-scattering spectra in $Nd_{0.5}Ca_{0.5}MnO_3$. The bands **d** and **e** are the JT and breathing mode, respectively. (b) Temperature dependences of the amplitudes for the coherent oscillations associated with oxygen atoms [A_i (i=2, 3, and 4)] and the intensities of the corresponding Raman bands (**b**, **c**, and **d**).

man process[22,23] but to the displacement-type coherent oscillations associated with the photoinduced melting of the charge and orbital order. The 469 cm^{-1} oscillation is seen to have a relatively large amplitude compared to the other three oscillations and dominates the main oscillatory structures in the initial response, as indicated by the vertical broken lines in Fig. 4(b).

To obtain information about the origin of the coherent oscillations, it is useful to refer to the results of Raman spectroscopy.[24–28] Figure 5(a) shows the temperature variation in Raman spectra for $Nd_{0.5}Ca_{0.5}MnO_3$. The polarizations of incident and scattered lights are perpendicular to the **c** axis and the direction of the incident and scattered lights is parallel to the **ab** plane. The results are almost identical to those previously reported by Jandl *et al.*,[26] although they did not measure the spectra below 100 cm^{-1}.

As seen in Fig. 5(a), no prominent bands are observed at 300 K. As the temperature decreases, new peaks **a**–**f** appear below T_{CO} and increase in intensity. These bands are activated by lattice distortion and/or atomic displacements associated with the charge and orbital order. The observed coherent oscillations correspond well to the four Raman bands, **a**(83 cm^{-1}), **b**(226 cm^{-1}), **c**(346 cm^{-1}), and **d**(484 cm^{-1}). Previous studies revealed that band **a** could be assigned to the vibration mode of A-site cations, and bands **b** and **c** to the rotational modes of MnO_6 octahedra shown in Fig. 6 [i] an6 [ii], respectively.[27,28] Band **d** was assigned to the JT mode shown in Fig. 6 [iii].[24] The observed coherent oscillations should have the same origins as these bands **a**–**d**. The tem-

TABLE I. Parameters obtained from the fitting procedure and the mode assignment of the observed coherent oscillations.

i	ω_i (cm^{-1})	$A_i(\times 10^{-4})$	τ_i (ps)	ϕ_i (rad)	Assignment
1	82	130	1.08	0.060π	A-site cation vibration
2	224	62	0.42	0.143π	Rotational mode of
3	339	25	0.79	-0.050π	MnO_6 octahedra
4	469	590	0.07	-0.095π	Jahn-Teller

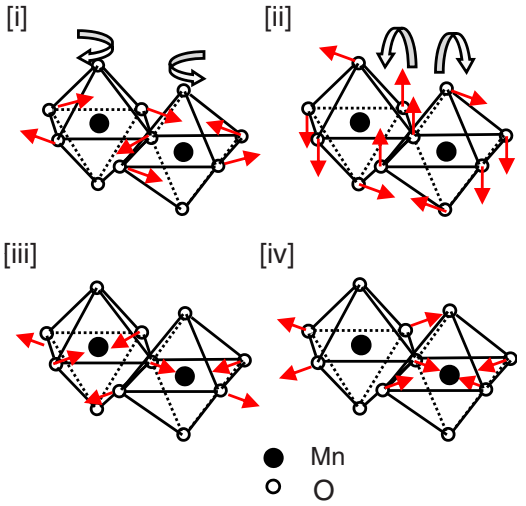

FIG. 6. (Color online) Schematic views of Raman modes: [i] and [ii] the rotational modes of MnO_6 octahedra, [iii] the JT mode, and [iv] the breathing mode. The bands **b**-**e** are assigned to modes [i]–[iv], respectively.

perature dependences of the amplitudes A_i (i=2, 3, and 4) for the three oscillations associated with oxygen atoms are plotted in Fig. 5(b), together with the integrated intensities of the Raman bands **b**–**d**. The temperature dependences of the amplitudes A_i (i=2, 3, and 4) and the intensities of Raman bands **b**–**d** are almost identical, consistent with our assignments.

Taking these assignments into account, the dynamics of the photoinduced melting of the charge and orbital order can be discussed. By photoirradiation, the charge order is first melted within the time resolution (~30 fs) via strong electron correlations. This is a purely electronic process and will occur in the time scale of the transfer energy (0.5 eV), that is, about 8 fs. In the present measurement system, therefore, only the instantaneous response was detected as shown in Fig. 3(a). When the charge order is melted, the atomic displacements, which stabilize the charge and orbital order, should be released, since they are not necessary for the non-charge-ordered state or equivalently the $Mn^{3.5+}$ state. In this case, it is reasonable that coherent oscillations, which correspond to the atomic displacements stabilizing the ordered phase, should be generated. Such coherent oscillations have previously been reported in other examples of photoinduced phase transitions.[29–35]

Here, let us briefly discuss semiquantitatively the amplitude of the coherent oscillation due to the JT mode, which is the largest among the four oscillations. As seen in the lower panel of Fig. 1(b), the state generated just after a photoirradiation is almost equal to the state at 230 K, at which the charge order is considerably weakened, as deduced from the very small intensity of the Raman band related to the charge order [see Fig. 5(b)]. Therefore, the charge order is almost melted by a photoirradiation of 0.01 ph/Mn in the case of Fig. 1(b) (the lower panel). In our experiments shown in Figs. 2 and 4, the excitation photon density is 0.0065 ph/Mn, smaller than 0.01 ph/Mn in Fig. 1(b) (the lower panel). Since the signal showing the melting of charge order is roughly

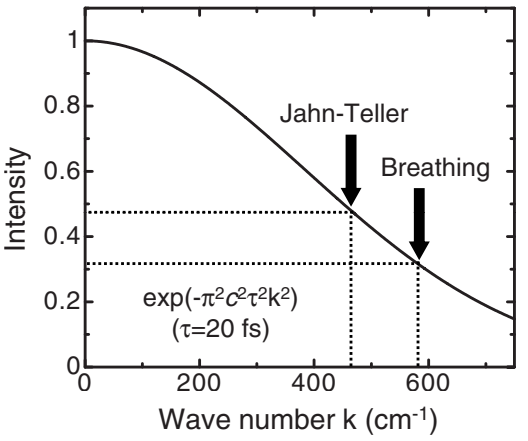

FIG. 7. The Fourier transform of the Gaussian response function $[\exp(-t^2/\tau^2)]$ in the measurement system $[\exp(-\pi^2c^2\tau^2k^2), \tau = 20$ fs], which corresponds to the wave-number dependence of the detection sensitivity for coherent oscillations.

proportional to the excitation photon density as shown in Fig. 3(b), it is reasonable to consider that one-photon excitation also destroys the charge order almost completely in a domain, the size of which was estimated to be about 140 Mn sites as mentioned above. The evaluated amplitude of the coherent oscillation (A_4) in $\Delta R_{\rm osc}/R$ due to the JT mode is 0.059 (see Table I), which is half of the background reflectivity change, $\Delta R/R \sim 0.12$ [see the lower panel of Figs. 2 and 3(b)]. This demonstrates that the initial amplitude of the atomic displacements in the coherent oscillation due to the JT mode is really large. Such a large coherent oscillation would be observed only in the photoinduced phase transition systems.

The large amplitude of the coherent oscillation A_4 suggests a strong coupling of the JT mode to the charge order. In general, the breathing mode shown in Fig. 6 (part iv),[24,25] which corresponds to the shrinking (or expanding) of the MnO_6 octahedra, is considered to couple strongly to charge order as well as the JT mode. The coherent oscillation of the breathing mode was, however, never observed. To ascertain the minor contribution of the breathing mode, we have to consider the limitation of the time resolution (~30 fs) and the resultant decrease in detection sensitivity of oscillations in our measurement system, since the frequency (585 cm^{-1}) of the breathing mode (the Raman band **e**) is relatively high and the period of the modes (57 fs) is close to the time resolution. The detection sensitivity of oscillations is given by the Fourier transform of the Gaussian response function, $\exp(-t^2/\tau^2)$, (τ=20 fs), which is shown in Fig. 7. As indicated by the arrows in Fig. 7, the amplitudes of the oscillations for the JT mode and the breathing mode are expected to be about half and one third of the original ones, respectively, indicating the sufficient sensitivity of the two modes. Consequently, the coherent oscillation of the breathing mode should be much weaker than that of the JT mode. Thus, we can conclude that the breathing mode is not so important for the stabilization of the CE-type charge and orbital order as compared to the JT mode.

As mentioned above, the charge order is melted by a photoirradiation and is recovered with a time constant of 0.6 ps.

If a phonon mode is strongly coupled to the charge order, the coherence of the oscillation due to the mode should be disturbed within 0.6 ps and the decay time of the oscillation is much shorter than 0.6 ps. In the oscillations of $i=1-3$, the decay time of the amplitudes, $\tau_1-\tau_3$, is 0.42–1.08 ps, which is comparable to 0.6 ps. This indicates that these oscillations are not strongly coupled to the charge order. On the other hand, the decay time of the oscillation due to the JT mode (τ_4) is very short, being 0.07 ps. Such a short decay time as well as a large amplitude of the coherent oscillation of the JT mode is unambiguous evidence of the fact that the JT mode is strongly coupled to the charge order. This means that the orbital order correlated directly with the JT mode plays a significant role in the stabilization of the charge order. The importance of the JT mode for the stabilization of the charge order has indeed been highlighted by several recent theoretical studies.[8–12]

We can now present the overall dynamics of the photoinduced melting of charge and orbital order as illustrated in Fig. 8. By photoirradiation, the charge order [Fig. 8(a)] is first melted within the time resolution (~30 fs) through a purely electronic process [Fig. 8(b)]. The oxygen displacements are subsequently released, accompanied by the coherent oscillations. The strong coupling of the JT mode with charge order gives rise to the large amplitude of the coherent oscillation due to the JT mode [Fig. 8(c)]. Recovery to the charge-order state [Fig. 8(a)] from the nonordered state [Fig. 8(d)] occurs with a time constant of 0.6 ps and the temperature of the system increases.

The ultrafast dynamics of the photoinduced melting of the charge order was previously reported for $Pr_{0.7}Ca_{0.3}MnO_3$ (Ref. 36). In that study, the melting of the charge order was found to occur over a time scale of ~50 fs, which is considerably different from our results. However, the data for $Pr_{0.7}Ca_{0.3}MnO_3$ were measured with $x_{ph}\sim 0.23$ ph/Mn, which is more than 1 order of magnitude higher than ours. Therefore, nonlinear and/or cooperative effects produced only by the strong excitation might give rise to the delayed responses.

IV. SUMMARY

Ultrafast charge and lattice dynamics during photoinduced melting of charge and orbital order in $Nd_{0.5}Ca_{0.5}MnO_3$ was investigated by pump-probe reflection measurements with a time resolution of ~30 fs. After photoirradiation, e_g electrons delocalize and then charge order is melted over ~140 Mn sites per photon. This process is purely electronic and occurs within 30 fs. Subsequently to this melting of the charge order, the displacements of oxygen atoms are released and the strong coherent oscillations of the Jahn-Teller mode are driven. These results demonstrate that the orbital order as well as the intersite Coulomb correlation plays a significant role in the stabilization of the charge-order phase. These findings will be important for deeper understanding of not only the stabilization mechanism of the charge-order phase but also the mechanism of the colossal magnetoresistance phenomena in perovskite-type manganites.

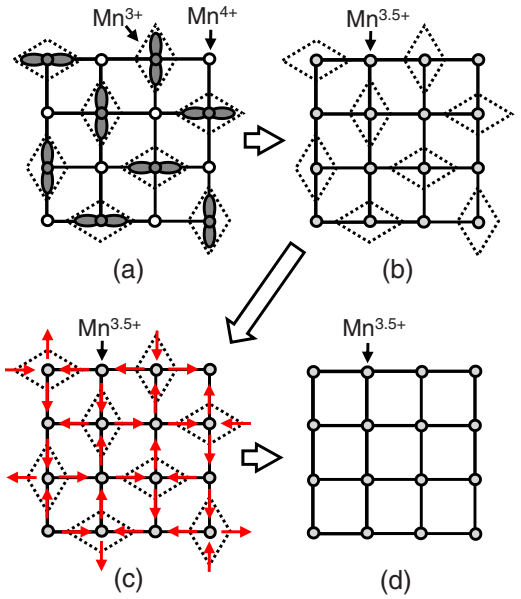

FIG. 8. (Color online) Schematics for the overall dynamics of photoinduced melting of charge and orbital order in $Nd_{0.5}Ca_{0.5}MnO_3$. (a) The charge- and orbital-order state. (b) The melting of the charge order by a photoirradiation. The JT distortions remain just after the photoirradiation. (c) The release of the JT distortion. In this process, the coherent oscillations of the JT mode are generated (not shown). (d) The nonordered state. Recovery to the charge- and orbital-order state occurs with the time constant of 0.6 ps and simultaneously, the temperature of the system is increased (not shown).

ACKNOWLEDGMENTS

The authors wish to thank A. Cavalleri for enlightening discussions. This work was supported in part by MEXT, Japan (Grants No. 16076207 and No. 20110005) and JPSJ (Grant No. 20340072).

*Present address: Division of Materials Physics, Graduate School of Engineering Science, Osaka University, Toyonaka, Osaka 560–8531, Japan.

†Corresponding author; okamotoh@k.u-tokyo.ac.jp

[1] A. Moreo, S. Yunoki, and E. Dagotto, Science **283**, 2034 (1999).

[2] M. Imada, A. Fujimori, and Y. Tokura, Rev. Mod. Phys. **70**, 1039 (1998).

[3] Y. Tokura, Rep. Prog. Phys. **69**, 797 (2006).

[4] J. B. Goodenough, Phys. Rev. **100**, 564 (1955).

[5] Y. Murakami, H. Kawada, H. Kawata, M. Tanaka, T. Arima, Y.

Moritomo, and Y. Tokura, Phys. Rev. Lett. **80**, 1932 (1998).
[6] J. van den Brink, G. Khaliullin, and D. Khomskii, Phys. Rev. Lett. **83**, 5118 (1999).
[7] T. Mutou and H. Kontani, Phys. Rev. Lett. **83**, 3685 (1999).
[8] T. Mizokawa and A. Fujimori, Phys. Rev. B **56**, R493 (1997).
[9] T. Hotta, A. L. Malvezzi, and E. Dagotto, Phys. Rev. B **62**, 9432 (2000).
[10] S. Yunoki, T. Hotta, and E. Dagotto, Phys. Rev. Lett. **84**, 3714 (2000).
[11] J. Bala, P. Horsch, and F. Mack, Phys. Rev. B **69**, 094415 (2004).
[12] Y. S. Lee, S. Onoda, T. Arima, Y. Tokunaga, J. P. He, Y. Kaneko, N. Nagaosa, and Y. Tokura, Phys. Rev. Lett. **97**, 077203 (2006).
[13] M. Fiebig, K. Miyano, Y. Tomioka, and Y. Tokura, Science **280**, 1925 (1998).
[14] M. Fiebig, K. Miyano, Y. Tomioka, and Y. Tokura, Appl. Phys. B: Lasers Opt. **B71**, 211 (2000).
[15] T. Ogasawara, T. Kimura, T. Ishikawa, M. Kuwata-Gonokami, and Y. Tokura, Phys. Rev. B **63**, 113105 (2001).
[16] T. Ogasawara, K. Tobe, T. Kimura, H. Okamoto, and Y. Tokura, J. Phys. Soc. Jpn. **71**, 2380 (2002).
[17] Y. Okimoto, H. Matsuzaki, Y. Tomioka, I. Kezsmarki, T. Ogasawara, M. Matsubara, H. Okamoto, and Y. Tokura, J. Phys. Soc. Jpn. **76**, 043702 (2007).
[18] D. Lim, V. K. Thorsmolle, R. D. Averitt, Q. X. Jia, K. H. Ahn, M. J. Graf, S. A. Trugman, and A. J. Taylor, Phys. Rev. B **71**, 134403 (2005).
[19] M. Matsubara, Y. Okimoto, T. Ogasawara, Y. Tomioka, H. Okamoto, and Y. Tokura, Phys. Rev. Lett. **99**, 207401 (2007).
[20] K. Tobe, T. Kimura, and Y. Tokura, Phys. Rev. B **69**, 014407 (2004).
[21] The errors between the experimental oscillatory signal and the calculated one can be evaluated by means of the chi-square test. In the case that the main oscillation with 469 cm^{-1} associated with the JT mode is assumed to be of sine type, the error is more than 1 order of magnitude larger than that in the fitting result shown in Fig. 4 and the fine structures seen in Fig. 4(b) cannot be reproduced well.
[22] L. Dhar, J. A. Rogers, and K. A. Nelson, Chem. Rev. (Washington, D. C.) **94**, 157 (1994).
[23] T. E. Stevens, J. Kuhl, and R. Merlin, Phys. Rev. B **65**, 144304 (2002).
[24] K. Yamamoto, T. Kimura, T. Ishikawa, T. Katsufuji, and Y. Tokura, Phys. Rev. B **61**, 14706 (2000).
[25] M. V. Abrashev, J. Backstrom, L. Borjesson, M. Pissas, N. Kolev, and M. N. Iliev, Phys. Rev. B **64**, 144429 (2001).
[26] S. Jandl, A. Mukhin, V. Yu. Ivanov, and A. M. Balbashov, J. Phys.: Condens. Matter **18**, 1667 (2006).
[27] V. A. Amelitchev, B. Guttler, O. Yu. Gorbenko, A. R. Kaul, A. A. Bosak, and A. Yu. Ganin, Phys. Rev. B **63**, 104430 (2001).
[28] M. N. Iliev, M. V. Abrashev, J. Laverdiere, S. Jandl, M. M. Gospodinov, Y. Q. Wang, and Y. Y. Sun, Phys. Rev. B **73**, 064302 (2006).
[29] A. Cavalleri, Th. Dekorsy, H. H. W. Chong, J. C. Kieffer, and R. W. Schoenlein, Phys. Rev. B **70**, 161102(R) (2004).
[30] H. Okamoto, Y. Ishige, S. Tanaka, H. Kishida, S. Iwai, and Y. Tokura, Phys. Rev. B **70**, 165202 (2004).
[31] H. Okamoto, K. Ikegami, T. Wakabayashi, Y. Ishige, J. Togo, H. Kishida, and H. Matsuzaki, Phys. Rev. Lett. **96**, 037405 (2006).
[32] S. Iwai, Y. Ishige, S. Tanaka, Y. Okimoto, Y. Tokura, and H. Okamoto, Phys. Rev. Lett. **96**, 057403 (2006).
[33] H. Matsuzaki, M. Yamashita, and H. Okamoto, J. Phys. Soc. Jpn. **75**, 123701 (2006).
[34] K. Ikegami, K. Ono, J. Togo, T. Wakabayashi, Y. Ishige, H. Matsuzaki, H. Kishida, and H. Okamoto, Phys. Rev. B **76**, 085106 (2007).
[35] K. Kimura, H. Matsuzaki, S. Takaishi, M. Yamashita, and H. Okamoto, Phys. Rev. B **79**, 075116 (2009).
[36] D. Polli, M. Rini, S. Wall, R. W. Schoenlein, Y. Tomioka, Y. Tokura, G. Cerullo, and A. Cavalleri, Nature Mater. **6**, 643 (2007).